Iranian Journal of Physics Research, Vol. 22, No. 3, 2022
DOI: 10.47176/ijpr.22.3.11404

Evaluation of the effect of different concentrations of boron on proton therapy of the liver using GEANT4 Monte Carlo toolkit

M Tatari [1]*, Z Hashemi[1], and H Naik [2]
1. Physics Department, Faculty of Science, Yazd University, Yazd 89195-741, Iran
2. Radiochemistry Division, Bhabha Atomic Research Centre, Mumbai 400085, India

E-mail: mtatari@yazd.ac.ir

(Received 27 January 2022 ; in final form 4 October 2022)

Abstract
Experimental results have shown that dadding boron to tumor tissue during proton therapy increases the mortality of cancer cells. This work has investigated how to form a spread-out Bragg peak in the proton therapy of a liver-located tumor by simulating the MIRD phantom and designing a range modulator. The simulations were carried out using a GEANT4 Monte Carlo toolkit. Also, the absorbed dose of the different organs near the liver was determined via simulations. To study the effect of boron on liver proton therapy, a tumor impregnated with different percentages of boron was simulated and the effect of energy released in the tumor as a result of alpha particles, protons and their combinations was investigated. The absorbed dose in the tumor at different proton energies and with varying percentages of boron was investigated. It was found that the absorbed dose in the tumor increases by adding boron, however; it decreases by increasing the energy from a certain limit (~80 MeV) of more than 60% boron.

Keywords: proton therapy of liver, Bragg peak, boron, alpha particles, GEANT4 toolkit.

1. Introduction

When protons pass through a substance, they interact with electrons and atomic nuclei via the Coulomb force. There is a rare possibility for collisions with atomic nuclei that cause nuclear interactions. However, these nuclear interactions produce secondary particles and lead to side effects in proton therapy. A key advantage of proton therapy is the localized energy release in an area referred to as the Bragg peak. Proton therapy technique primarily relies on the ability of the manipulation of the Bragg peak. The Columbic interactions have the largest contribution to the production of Bragg peak. However, nuclear reactions can also be used to make protons more effective in proton therapy. Proton therapy can be employed to treat large tumors in such a way that healthy tissues do not receive radiation as much as possible. Bragg peaks can be created in different depths by passing proton beams through a range modulator with different thicknesses. A spread-out Bragg peak (SOBP) can be produced via their integration and therefore large tumors can be covered [1-4]. Proton therapy can treat various cancers such as, brain, lung, liver, etc. with slightly damaging surrounding organs [5-8].

Clinical studies of liver cancer proton therapy have indicated that the application of protons to treat liver cancer is effective, so that it is found in a clinical study on 133 patients (each received a dose of approximately 70 Gy during the treatment period) that none of the patients died as a result of liver dysfunction, and the results of this study suggest the application of proton therapy for patients whose liver volume has decreased due to multiple or large lesions [9]. Since the dose received by healthy tissues around the tumor is low, the risk of secondary cancer that can happen after proton therapy is negligible. However, other strategies are required to reduce the administered dose [10].

Proton therapy benefits nuclear reactions in addition to atomic phenomena. Recent studies have shown that the presence of boron in the tumor area can increase the amount of absorbed dose by the tissue. Protons can interact with ^{11}B according to the following reaction [11]:

$$^{11}B + p \rightarrow {}^{12}C \rightarrow {}^{8}Be + \alpha \rightarrow 3\alpha + 8.7\ MeV$$

Experimental results clearly indicate that the proton-boron nucleus reaction is a nuclear reaction resulting in

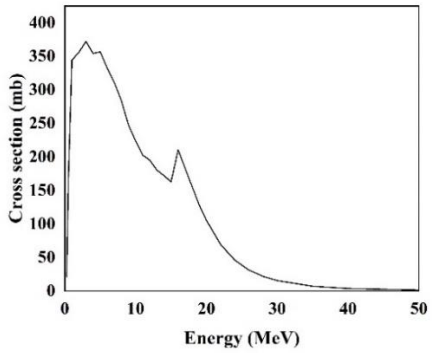

Figure 1. Cross section of $^{11}B(p,\alpha)$ reaction, data from TENDL 2021 [16].

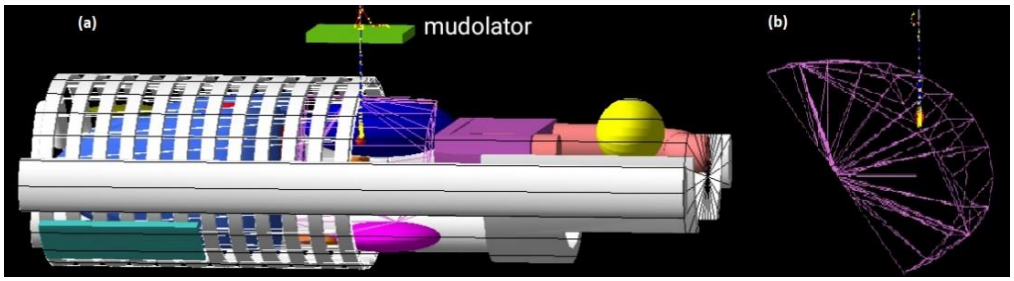

Figure 2. (a) MIRD Phantom and range modulator and (b) Liver and proton beam.

the production of three alpha particles having low energy (less than 4 MeV) and, as a result, high linear energy transfer (high-LET) [12,13]. The probability of this reaction increases around the Bragg peak leading to an increase in the absorbed dose at this depth [14,15]. Cross section of this reaction is shown in figure 1 [16]. Cells were irradiated with a proton beam in the presence of sodium borocaptate ($Na_2B_{12}H_{11}SH$ or "BSH"), which is a common agent clinically used in BNCT in its ^{10}B-enriched form to selectively deliver given boron concentrations in cancer cells. In order to maximize the $p + {}^{11}B \rightarrow 3\alpha$ reaction rate, BSH was used with naturally occurring boron isotopic abundance [11]. The advantage of using proton therapy compared to the Boron Neutron Capture Therapy (BNCT) is that in BNCT, the thermal neutrons interact with ^{10}B isotopes, and the abundance of ^{10}B is 20%, while in proton therapy, the protons interact with ^{11}B isotopes and the abundance of ^{11}B is 80%. On the other hand, three alpha particles are produced in a boron-proton interaction, but in a boron-neutron interaction, one alpha particle is produced, making proton therapy more effective in the presence of boron. The simulation results show that the increase of dose in the Bragg peak region cannot be related to the alpha particles due to their small number of productions. With the rise of energy deposition, the absorbed dose increases in the Bragg peak region [17]. However, the presence of alpha particles with high linear energy transfer cannot be ignored. Experimental results indicate that the existence of boron and the production of alpha particles increase the rate of damage to the target tissue (tumor) [18].

The present study aims to evaluate the absorbed dose in healthy regions around the tumor and the surrounding organs via the simulation of liver proton therapy. To do this, a tumor inside the liver was simulated and the amount of absorbed dose in the presence and absence of boron was calculated. The simulations were performed using the GEANT4 code.

2. Materials and methods

Proton deposits a small dose on its way when it enters the body. Increasing the depth and reducing the speed increases the absorbed dose in the tissue. The protons are stopped at the end of the proton range, albeit the absorbed dose rises to a peak. It is called the Bragg peak. The beam can be adjusted to place Bragg peak at the tumor site. The width of the Bragg peak is not enough to cover large tumors. The proton energy is changed by passing the beam through a range modulator, and many Bragg peaks occur at various depths. The spread-out Bragg peak was obtained from the superposition of multiple Bragg peaks [5]. With increasing the thickness of the range modulator, the created Bragg peaks cover the entire tumor volume. The thickness of the poly-methyl methacrylate changes from 0 to 4.2 mm in 7 steps, meaning that the thickness increases by 0.7 mm at each step. The spread-out Bragg peak was obtained by using the superposition of pristine Bragg curves with different weight coefficients. Bragg curves were assembled according to the following relation [19]:

$w_1D_{1i}+w_2D_{2i}+\ldots+ w_ND_{iN}=D_0 \qquad i=1, 2, \ldots, N,$

where w_i parameters are the weight coefficients, which are dimensionless and calculated using MATLAB software. D_i parameters are the proton dose at each Bragg curve at a certain depth. D_0 is a constant value related to the amount of dose in the SOBP region. N is the number of equations representing the number of pristine Bragg curves. A MIRD phantom was utilized in this study [20], as shown in figure 2. Table 1 lists the

Table 1. Materials used in simulation and their mass percentage [20].

	H	C	N	O	Na	P	S	Cl	K	Ca	Density(g/cm³)
Liver	10.3	11.5	2.2	75.1	0.1	0.1	01	02	0.1	-	1.079
Heart	10.4	13.9	2.9	71.8	0.1	0.2	0.2	0.2	0.3	-	1.081
Pancreas	10.6	16.9	2.2	69.4	0.2	0.2	0.1	0.2	0.2	-	1.087
Stomach	10.6	11.5	2.2	75.1	0.1	0.1	0.1	0.2	0.1	-	1.088
Spleen	10.3	11.3	3.2	74.1	0.1	0.3	0.2	0.2	0.3	-	1.089
Lung	10.3	10.5	3.1	74.9	0.2	0.2	0.3	0.3	0.2	-	0.296
Kidney	10.3	13.2	3.0	72.4	0.2	0.2	0.2	0.2	0.2	0.1	1.066
Adrenal	10.5	25.6	2.7	60.2	0.1	0.2	0.3	0.2	0.2	-	1.028

Table 2. Range modulator specifications.

Thickness(mm)	Beam Weight
0	4.148
0.7	1.499
1.4	1.149
2.1	0.979
2.8	0.850
3.5	0.737
4.2	0.674

materials defined in the phantom [20]. A spherical tumor was designed with a radius of 0.5 cm in the liver to investigate its cancer. A proton surface source with a radius of 0.5 cm at a distance of 25 cm from the center of the tumor was considered and designed so that the proton beams are normally incident to the abdomen. The proton beam must pass through a 1 cm diameter tumor in this situation,. The source energy of 84 MeV is considered so that the depth of the Bragg peak is located at the end of the tumor. Then, a thin poly-methyl methacrylate was placed between the source and the phantom as a range modulator to obtain the thickness of each range modulator step. Resulting in a range modulator with 0.7 mm thick steps that add up to a thickness of 4.2 mm, for which, the Bragg peak is located at the beginning of the tumor. The range modulator information is shown in table 2. The simulations were performed using the GEANT4 Monte Carlo toolkit with 10^7 histories. GEANT4 is a versatile C++ Monte Carlo simulation toolkit that simulates all kinds of particles. The G4V User Detector Construction class was used to design the geometry. The G4 Material class was used to define the material in accordance with table 1. The simulations utilized the QGSP_BERT physical reference. The processes involved in this physics are given in [21]:

1. Hadronic component: The purely hadronic part of this physics list consists of elastic, inelastic, capture and fission processes. Each process is built from cross section sets and interaction models that provide the detailed physics implementation.

Inelastic models: The inelastic hadron-nucleus processes are implemented by the quark-gluon model (QGS), the Fritiof parton model (FTF), Bertini and Precompound models.

Inelastic cross sections: G4BGGNucleonInelasticXS is used for protons, G4NeutronInelasticXS for neutrons, and G4BGGPionInelasticXS for pions. In these cross-sections Barashenkov parameterization is used below 91 GeV and Glauber-Gribov above.

Elastic models: Elastic scattering of protons and neutrons use G4ChipsElasticModel from 0 to 100 TeV. This model uses the Kossov parameterized cross sections.

Elastic cross sections: 4BGGNucleonElasticXS is used for protons, G4NeutronElasticXS for neutrons, and G4BGGPionElasticXS for pions. In these cross sections Barashenkov parameterization is used below 91 GeV and Glauber-Gribov above.

Capture and stopping: Neutron capture uses the G4NeutronRadCapture model with the G4NeutronCaptureXS cross sections. Muon capture or decay at rest is handled by the G4MuonMinusCapture process.

2. Electromagnetic component: This physics list uses "standard" GEANT4 electromagnetic physics as built by the G4EmStandardPhysics constructor. It is implemented for γ, $e-$, $e+$, $\mu-$, $\mu+$, $\tau-$, $\tau+$, and all stable charged hadrons/ion. There is no treatment of optical photons in this physics list, optical physics should be added on top of any reference or user custom physics.

3. Decay component: The decay of all long-lived hadrons and leptons is handled by the G4Decay process. It does not handle the decay of hadronic resonances like deltas, which should be decayed within hadronic models and heavy-flavor particles like D and B mesons or charmed hyperons. Muon capture or decay at rest is handled by the G4MuonMinusCapture process.

4. Neutron tracking cut: Neutrons may be killed by energy or time cut.

G4 General Particle Source class was used to simulate the source and generate the primary particles (protons). This class allows users to define spectral sources and sources with different spatial distributions. The physical reference QGSP INCLXX was used to transport particles into matter and to consider interactions and production of secondary particles. This physical reference is for interactions involving protons and neutrons with less than 3 GeV energy. It is based on experimental information and has been proposed for medical and industrial applications. Geant4.10.07 version is used in this paper.

Researches have shown that the presence of the boron isotope ^{11}B in targets improves the effectiveness of proton therapy [22]. The addition of boron to the tumor tissue is simulated as a mixture, and its density is calculated from the following equation:

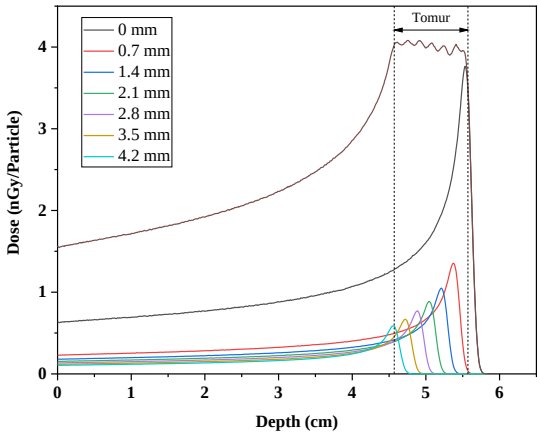

Figure 3. Depth-dose distribution of a spread-out Bragg peak with a range modulator.

Table 3. The D2 and D98 in tumor with different concentrations of ^{11}B.

nGy/proton	0%	20%	40%	60%	80%	100%
D2	74.73	75.18	75.30	75.69	75.4	75.17
D98	1.35	1.41	1.45	1.47	1.21	1.14

Table 4. Absorbed dose by different phantom organs.

Organ	Dose(nGy/Particle)
Tumor	0.024386 ±0.000163
Soft liver tissue	0.005054 ±0.000018
Heart	0.000249 ±0.000001
Pancreas	0.000885 ±0.000002
Stomach	0.000579 ±0.000002
Spleen	0.000176 ±0.000001
Right Lung	0.000345 ±0.000002
Left Lung	0.000236 ±0.000002
Right Kidney	0.001070 ±0.000018
Left Kidney	0.000253 ±0.000002
Right Adrenal	0.000046 ±0.0000001
Left Adrenal	0.000481 ±0.000002

$$\rho_m = \frac{100}{\left[\left(100-c_b\right)\rho_t + c_b\rho_b\right]},$$

where,refers ρ_t tes the density of the mixturedicain ρ_m to the density of healthy tissue, ρ_b is the boron density equal to 2.38 g/cm^3 , and c_b shows the boron concentration [23].

In this paper, a tumor inside the liver was simulated and the amount of absorbed dose in the presence of different percentages of boron, and absence of boron was calculated (Figure 6 and Table 5). Also, the effect of using a modulator when different concentrations of boron are added to the tumor has been investigated (Table 5). The absorbed dose due to alpha particles resulting from boron-proton interaction in the tumor and healthy tissues around the liver has been calculated (Figure 4).

3. Results

The results of using the range modulator to form Bragg peaks are shown in figure 3. As can be seen, the produced SOBP covers the 1-cm tumor. Due to the tumor irradiation, a certain dose is absorbed into the tissues around the tumor, where the highest amount isresulting from the released energy of secondary particles. The absorbed dose at 2% of the target volume and the absorbed dose at 98% of the target volume are called D2 and D98, respectively. Table 3 shows the D2 and D98 results in the tumor with different percentages of boron. The absorbed dose by the 10 sensitive body organs near the liver, as well as the dose of incident protons and secondary particles in the liver tumor and healthy tissue, are shown in table 4. As can be seen, the highest dose is absorbed by the tumor, and the other mentioned organs have a negligible absorbed dose.

In the next step, different percentages of ^{11}B (0%, 20%, 40%, 60%, 80%, and 100%) were added to the tumor tissue to investigate the effect of boron. Figure 4 shows the energy released to the tumor tissue resulting from the alpha particles, the protons, and the total energy deposition with different percentages of boron.

As it can be seen from figure 4, the energy released from the alpha particles increases by increasing the boron percentage, although its amount is negligible. It can be seen that the percentage of the energy deposition of alpha particles in the tumor is 1.43%, 1.75%, 2.08%, 2.54%, 2.76% and 3.19% of the total

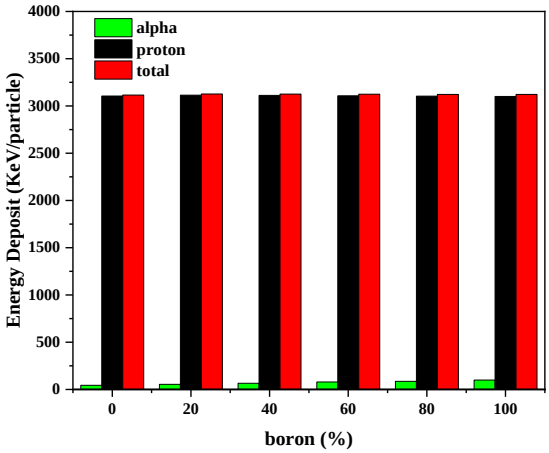

Figure 4. Energy deposition into tumor tissue in the presence of different percentages of ^{11}B.

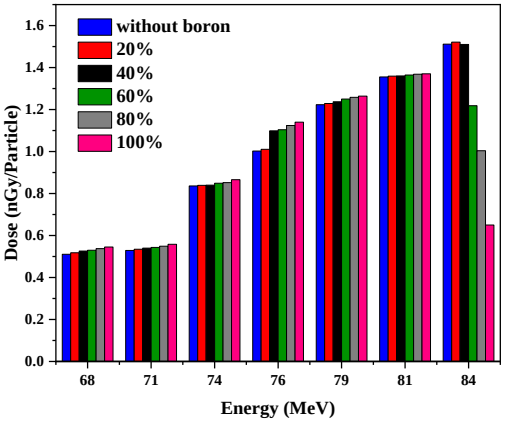

Figure 5. Absorbed dose in the tumor at different proton energies and with different percentages of ^{11}B.

energy released in the tumor for the presence of 0%, 20%, 40%, 60%, 80% and 100% boron concentration in the tumor tissue, respectively.

Figure 5 indicates the absorbed dose of the tumor at different proton energies and with varying percentages of boron. The results show that the absorbed dose in the tumor for 68 MeV protons varies from 0.510745 nGy/proton when boron is not used, to 0.54519 nGy/proton when 100% of the tumor is boron.

This means that the absorbed dose is increased by 6.7%. This value for 71 MeV protons is from 0.528684 nGy/proton to 0.55819nGy/proton (5.58% increase), for 74 MeV protons from 0.836007 nGy/proton to 0.865903 nGy/proton (3.58% increase), for 76 MeV protons from 1.00221 nGy/proton to 1.140029 nGy/proton (13.75% increase), for 79 MeV protons from 1.22312 nGy/proton to 1.26381 nGy/proton (3.32% increase) and for 81 MeV protons from 1.35524 nGy/proton to 1.369971 nGy/proton (1.07% increase). For 84 MeV, protons with increasing the boron concentration from 0 to 20%, the absorbed dose in the tumor increases, and with increasing the boron concentration from 20% to 100%, a significant decrease in the absorbed dose in the tumor is observed.

The simulation data of absorbed dose by different organs with different percentages of boron are shown in table 5. It can be seen that the absorbed dose in the liver is higher than in the other organs. Figure 6 shows the absorbed dose caused by all types of secondary particles, such as neutron and gamma radiation, in different tissues for different boron percentages of tumor tissue. The statistical errors of all simulations are less than 2%.

4. Discussion

The effect of the presence of boron atoms causes the increase of the absorbed dose in the Bragg peak region, which has been confirmed in the simulations [15,16,17,21]. However, the effect for the addition of boron to the tumor tissue on the absorbed dose into the surrounding tissues needs to be investigated. As can be seen in figure 3, the depth-dose diagram of a spread-out Bragg peak indicates that the designed range modulator and the proton beam energy are suitable for the simulated liver tumor treatment. The results indicate that when the amount of boron in the tumor increases, the number of alpha particles is elevated. Thus, the energy released in the tumor tissue increases, which is negligible.

As can be seen in figure 5, the dose increases with an increase in the amount of boron in the tumor tissue, except at high energies where the increase in boron causes a decrease in dose due to the increase in the density and passage of 84 MeV proton beams throughout the tumor.

Experimentally it is not possible to fill the entire

Table 5. Absorbed dose by different phantom organs with different concentration of ^{11}B.

	Absorbed dose (nGy/particle)					
Organ	0%	20%	40%	60%	80%	100%
Tumor	0.024386 ±0.000163	0.025052 ±0.000195	0.025075 ±0.000143	0.025089 ±0.000116	0.024959 ±0.000193	0.024702 ±0.000199
Soft liver tissue	0.005054 ±0.000018	0.005054 ±0.000019	0.005054 ±0.000019	0.005054 ±0.000017	0.005055 ±0.000016	0.005059 ±0.000019
Heart	0.000249 ±0.000001	0.000260 ±0.000002	0.000277 ±0.000002	0.000278 ±0.000001	0.000332 ±0.000002	0.000336 ±0.000002
Stomach	0.000579 ±0.000002	0.000554 ±0.000002	0.000556 ±0.000002	0.000638 ±0.000002	0.000626 ±0.000002	0.000693 ±0.000002
Spleen	0.000176 ±0.000001	0.000168 ±0.000002	0.000227 ±0.000001	0.000151 ±0.000002	0.000240 ±0.000001	0.000175 ±0.000002
Right lung	0.000345 ±0.000002	0.000342 ±0.000001	0.000352 ±0.000002	0.000412 ±0.000002	0.000441 ±0.000002	0.000434 ±0.000002
Left lung	0.000236 ±0.000002	0.000217 ±0.000002	0.000273 ±0.000002	0.000265 ±0.000002	0.000259 ±0.000002	0.000273 ±0.000002
Pancreas	0.000885 ±0.000002	0.000966 ±0.000001	0.001004 ±0.000011	0.001323 ±0.000019	0.001704 ±0.000015	0.001823 ±0.000016
Right kidney	0.001070 ±0.000018	0.001327 ±0.000018	0.001277 ±0.000016	0.001510 ±0.000014	0.001302 ±0.000021	0.001568 ±0.000019
Left kidney	0.000253 ±0.000002	0.000228 ±0.000002	0.000474 ±0.000002	0.000432 ±0.000002	0.000434 ±0.000002	0.000458 ±0.000002
Right adrenal	0.000046 ±0.0000001	0.000035 ±0.0000001	0.000163 ±0.000001	0.000371 ±0.000002	0.000060 ±0.0000001	0.000060 ±0.0000001
Left adrenal	0.000481 ±0.000002	0.000421 ±0.000002	0.000402 ±0.000001	0.000418 ±0.000002	0.000413 ±0.000001	0.000451 ±0.000002

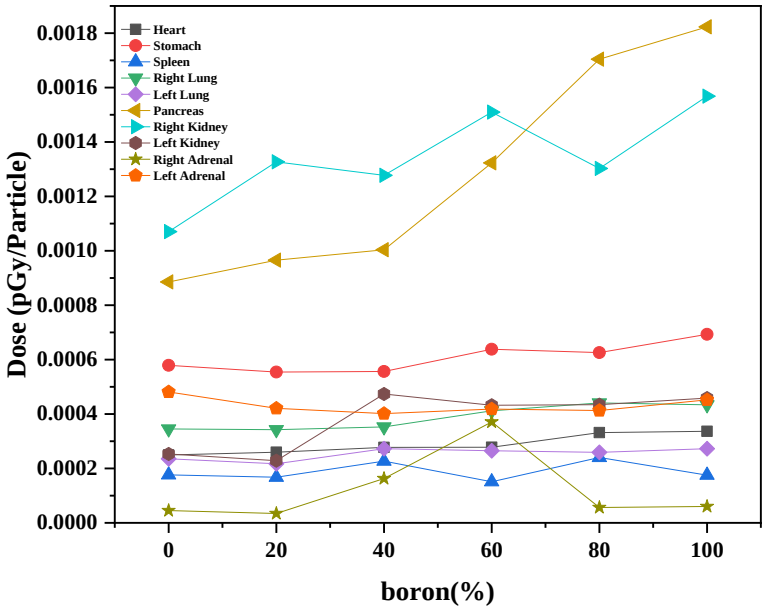

Figure 6. Absorbed dose in different phantom tissues with different percentages of ^{11}B in the tumor.

tumor volume with boron or to increase the boron content up to 60% or 80% of the tumor. The dose reduction in the energy of 84 MeV cannot be a reason for the weakness of proton therapy in the presence of boron.

It can be seen in figure 6, the absorbed doses of different tissues have not been significantly elevated, except for the pancreas and right kidney tissues, where this dose increase can be attributed to the proximity of the above two organs to the liver. Since this increase happens for of 60% and higher boron, it can be ignored.

The simulation results show that the dose delivered by protons is several orders of magnitude higher than that delivered by alpha particles [22]. Our results and other researches show that alpha particles produced by $p + {}^{11}B \rightarrow 3\alpha$ reaction are not responsible for increasing the biological effectiveness in the treatment of proton-boron fusion therapy.

5. Conclusions

According to the results, the increased amount of boron in the tumor tissue has negligible effect on the absorbed dose by the organs around the liver. The simulation results with GEANT4 code show that the application of

boron during the proton therapy can be helpful. It can be concluded that the presence of 60% to 80% of boron inside the liver tissue can be useful due to the increase of absorbed dose inside the liver tissue, and the results show that the highest amount of D2 and D98 is for the presence of 60% of boron in the liver tissue, therefore adding 60% boron is recommended for the treatment of liver tumor.

References

1. T Pawlicki, D Scanderbeg, and G Starkschall, "*Hendee's Radiation Therapy Physics*", Wiley (2016).
2. P Mayles, A Nahum, and J Rosenwald, "*Hand book of radiotherapy physics*" Taylor & Francis (2007).
3. S B Jia, *et al., Rep. pract. Oncol. Radiot.* **19** (2014) 376.
4. T Bortfeld, *Mad. Physi*. **24** (1997) 2024.
5. Z Hashemi, M Tatari, and H Naik, *Rep. pract. Oncol. Radiot*. **25** (2020) 927.
6. F Fracchiolla, *et al., Radiot. Oncol*. **154** (2021) 137.
7. E B Villarroel, X Geetsa, and E Sterpina, *Phys. Imag. Radiat. Oncol*. **15** (2020) 30.
8. S Mangan and M Leech, *Tech. Innov. Patient. Support. Radiat. Oncol*. **11** (2019) 1.
9. N Fukumitsu, *et al., Radiot. Oncol*. **117** (2015) 322.
10. R Yeung, *et al., Pract. Radiat. Oncol*. **8** (2018) 287.
11. G A P Cirrone, *et al., Scient. Rep*. **8** (2018) 1.
12. H W Becker, C Rolfs, and H P Trautvetter, *Atom. Nucl*. **327** (1987) 341.
13. G A P Cirrone, *et al., Med. Phys*. **3** (2018) 147.
14. F A Geser and M Valente, *Appl. Radiat. Isotop*. **151** (2019) 96.
15. D K Yoon, J Y Jung, and T S Suh, *Appl. Phys. Lett*. **105** (2014) 223507.
16. A J Koning, et al., Nucl. Data Sheets (2021).
17. T A Chiniforoush, *et al., Appl. Radiat. Isotop*. **170** (2021) 109596.
18. D Mazzucconi, *et al., Phys. Med*. **89** (2021) 226.
19. S B Jia, *et al., Nucl. Instrum. Methods Phys. Res.* A*: Accel. Spectrom. Detect. Assoc. Equip.* **806** (2016) 101.
20. J Valentin, *ICRP Rport* 89 (2002)
21. Geant4: *A Simulation Toolkit, Physics Reference Manual for Geant4*. CERN (2015).
22. H J Meyer, U Titt, and R Mohan, *Med. Phys*. (2022) 579.
23. Z Ahmadi Ganjeh and M Eslami-Kalantari, *Nucl. Instrum. Methods Phys. Res.* A*: Accel. Spectrom. Detect. Assoc. Equip*. **977** (2020) 164340.